Dimethylsilylbis(1-indenyl) Zirconium Dichloride/ Methylaluminoxane Catalyst Supported on Nanosized Silica for Propylene Polymerization

Kuo-Tseng Li, Fu-Sheng Ko

Department of Chemical Engineering, Tunghai University, Taichung, Taiwan, Republic of China

Received 1 January 2007; accepted 25 July 2007
DOI 10.1002/app.27152
Published online 10 October 2007 in Wiley InterScience (www.interscience.wiley.com).

ABSTRACT: A dimethylsilylene-bridged metallocene complex, $(CH_3)_2Si(Ind)_2ZrCl_2$, was supported on a nanosized silica particle, whose surface area was mostly external. The resulting catalyst was used to catalyze the polymerization of propylene to polypropylene. Under identical reaction conditions, a nanosized catalyst exhibited much better polymerization activity than a microsized catalyst. At the optimum polymerization temperature of 55°C, the former had 80% higher activity than the latter. In addition, the nanosized catalyst produced a polymer with a greater molecular weight, a narrower molecular weight distribution, and a higher melting point in comparison with the microsized catalyst. The nanosized catalyst's superiority was ascribed to the higher monomer concentration at its external active sites (which were free from internal diffusion resistance) and was also attributed to its much larger surface area. Electron microscopy results showed that the nanosized catalyst produced polymer particles of similar sizes and shapes, indicating that each nanosized catalyst particle had uniform polymerization activity. © 2007 Wiley Periodicals, Inc. J Appl Polym Sci 107: 1387–1394, 2008

Key words: metallocene catalysts; nanotechnology; poly (propylene); (PP); silicas; supports

INTRODUCTION

Polypropylene (PP) is one of the most important thermoplastics. It has a wide range of current uses and large potential for new applications such as thin films, fibers, blends, and composites.[1–3] Commercial isotactic PP is traditionally produced in a continuous slurry reactor or in a gas fluidized bed reactor with $MgCl_2$-supported Ziegler–Natta catalysts.

Metallocene-based catalyst systems have much higher activity and lower polydispersity than traditional Ti-based Ziegler–Natta catalysts.[4] In 1985, Kaminsky et al.[5] discovered the production of isotactic PP by a homogeneous metallocene catalyst [an ethylidene-bridged zirconocene complex, racemic $(C_2H_4)(Ind)_2ZrCl_2$, activated with methylaluminoxane (MAO)]. Since then, numerous studies have been performed to optimize polymerization performances of *ansa*-metallocene polymerization catalyst systems. Optimization targets have included higher activity/stereospecificity of the systems and desired high-molecular-weight polymers.

For *ansa*-metallocene polymerization catalysts, the size and type of the bridge connecting cyclopentadienyl (or indenyl) rings affect opening on the opposite side of the transition metal and, consequently, the relative rates of elementary steps in the polymerization mechanism.[6] Dimethylsilylene-bridged metallocene catalysts comprise some of the most commonly studied types of *ansa*-metallocene catalysts.[7] It has been found that the homogeneous catalyst dimethylsilylbis(1-indenyl) zirconium dichloride/methyl aluminoxane [$Me_2Si(Ind)_2ZrCl_2$/MAO)] is able to produce PP with a significantly higher molecular weight, melting point, and isotacticity in comparison with the catalyst $Et(Ind)_2ZrCl_2$/MAO under identical reaction conditions.[8]

Supported metallocene catalysts are preferred for the production of isotactic PP on an industrial scale because they can solve the problems observed with the soluble homogeneous catalysts (including the difficulty in controlling the polymer morphology, the very large amount of MAO needed, and the reactor-fouling problem).[9–15] Silica is one of the most frequently used supports because it leads to good morphological features for polymer particles. The most common method for preparing silica-supported metallocene catalysts is to treat the support with MAO first and then adsorb the metallocene on it.[14] In the literature, the sizes of the silica particles used to support metallocene/MAO catalysts for propylene polymerization to PP have usually been in the range of

Correspondence to: K.-T. Li (ktli@thu.edu.tw).
Contract grant sponsor: National Science Council of the Republic of China; contract grant number: NSC-94-2214-E029-002.

micrometers. For example, several microsized silicas have been used to support the $Me_2Si(Ind)_2ZrCl_2$/MAO catalyst for propylene polymerization.[16–20]

Nanosized silica particles have a very large external specific surface area. Recently, we used a nanosized silica as a support for the catalyst $(C_2H_4)(Ind)_2ZrCl_2$/MAO and found that a nanosized catalyst exhibited higher propylene polymerization activity than a microsized catalyst.[21] However, the molecular weight and isotacticity of PP produced by the nanosized-silica-supported $(C_2H_4)(Ind)_2ZrCl_2$/MAO catalyst were not high enough, probably because of the smaller rigidity of the ethylidene bridge in $(C_2H_4)(Ind)_2ZrCl_2$/MAO [compared with the Me_2Si bridge in $Me_2Si(Ind)_2ZrCl_2$].[7]

In this study, we used an MAO-treated nanosized silica particle to support $Me_2Si(Ind)_2ZrCl_2$ for propylene polymerization. In comparison with the microsized catalyst, the nanosized $Me_2Si(Ind)_2ZrCl_2$/MAO catalyst not only exhibited significantly better propylene polymerization activity but also produced PP with a significantly larger molecular weight and higher melting point when the polymerization temperature was greater than 40°C.

EXPERIMENTAL

Catalyst preparation and characterization

Two silica sources were used for supporting the $Me_2Si(Ind)_2ZrCl_2$/MAO catalyst. One silica was nanosized and was supplied by SeedChem (Melbourne, Australia); another silica was microsized and was supplied by Strem (Newburyport, MA). The silica-supported metallocene/MAO catalysts were prepared with a method reported before[22] according to the following procedure: (1) calcination of silica particles at 450°C under a nitrogen flow (100 mL/min) for 3 h, (2) immobilization of MAO on the supports by the heating and agitation of 3.5 mL of a 10 wt % MAO solution (in toluene) with 0.5 g of silica particles at 50°C for 24 h followed by washing and agitation with toluene three times, (3) reaction of the MAO-treated supports with 0.036 g of *rac*-$Me_2Si(Ind)_2ZrCl_2$ at 50°C for 16 h followed by washing and agitation with toluene three times, and (4) drying of the catalysts at 50°C. The operations of steps 2–4 were carried out under a dry argon atmosphere with the Schlenk technique. *rac*-$Me_2Si(Ind)_2ZrCl_2$ and MAO (10 wt % solution in toluene) were supplied by Strem and Albemarle (Baton Rouge, LA), respectively.

The specific surface areas of the silica samples were determined by nitrogen adsorption at the temperature of liquid nitrogen with a Micromeritics model ASAP 2020 Brunauer, Emmett, Teller (BET) surface area analyzer (Norcross, GA). The zirconium and aluminum contents of the supported metallocene/MAO catalysts were determined with an inductively coupled plasma/atomic emission spectrometer (model S-35, Kontron, Munich, Germany) after HF acid digestion of the solid.

Propylene polymerization and polymer characterization

A 100-mL, high-pressure autoclave reactor (supplied by Parr Instrument Co., Moline, IL) equipped with an impeller and a temperature control unit was employed for carrying out the catalytic polymerization of propylene. In a typical experiment, 50 mL of anhydrous toluene (water content $<$ 10 ppm; Aldrich, St. Louis, MO), 0.01 g of the supported *rac*-$Me_2Si(Ind)_2ZrCl_2$/MAO catalyst prepared by the impregnation method mentioned previously, and then a 0.4-mL MAO solution were charged into the reactor. The reactor was heated to the desired temperature. Propylene at 100 psi was then introduced into the reactor to initiate the polymerization, and the propylene pressure was kept constant at 100 psi. The agitator speed was set at 500 rpm, and the reaction time was 2 h, unless specified otherwise. A agitator speed of 500 rpm should be enough to eliminate external mass transfer resistance because no significant difference in the polymerization results was observed when the agitator speed was greater than 350 rpm. The polymerization was then terminated by the addition of acidic methanol, and the polymer product was dried in a vacuum oven. The experimental results were highly reproducible under identical reaction conditions.

The polymers produced were characterized with X-ray diffraction (XRD), scanning electron microscopy (SEM), optical microscopy, differential scanning calorimetry (DSC), solution viscometry, gel permeation chromatography (GPC), and ^{13}C-NMR. The polymer particle morphology was observed with a scanning electron microscope (JSM-6700F, JEOL, Tokyo, Japan). The polymer crystal structure was examined by XRD crystallography on a Shimadzu XRD-6000 diffractometer (Kyoto, Japan) with Cu Kα radiation. DSC measurements for the determination of the polymer melting point were carried out on a differential scanning calorimeter (Pyris 1, Perkin-Elmer, Waltham, MA) at a heating rate of 10°C/min. The structure of the melt-crystallized polymer was observed with an optical microscope (E400, Nikon, Tokyo, Japan) in cross-polarized light. The fraction of *mmmm* pentads in the polymer was evaluated from quantitative ^{13}C-NMR spectra, which were recorded with a Varian Unity-600 NMR spectrometer (Palo Alto, CA) at 100°C with *o*-$C_6D_4Cl_2$ as the solvent. The polymer molecular weight was determined with the solution viscosity method. The intrinsic viscosity ([η]) of the dried polymer was measured with a Schott AVS 300 system (Hofheim, Germany) at 135°C with *o*-$C_6H_4Cl_2$ as the solvent. The viscosity-

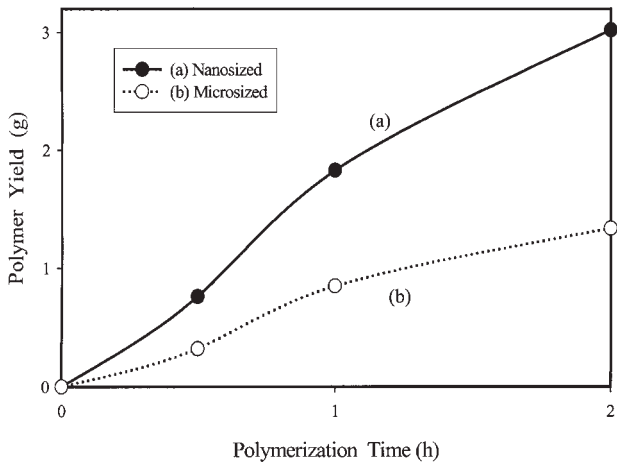

Figure 1 Polymer yield as a function of the reaction time for (a) nanosized and (b) microsized catalysts.

average molecular weight (M_v) was calculated from the [η] data with the Mark–Houwink equation ([η] = KM_v^{α}) for isotactic PP with $K = 1.3 \times 10^{-4}$ dL/g and $\alpha = 0.78$.[23] The molecular weight distributions (MWDs) were determined by high-temperature GPC with a Waters Alliance GPCV20000 system (Milford, MA) equipped with three columns (two Styragel HT6E and one Styragel HT2) at 135°C. *o*-Dichlorobenzene was used as the mobile phase.

RESULTS AND DISCUSSION

Effect of the polymerization time

Figure 1 shows the PP yield as a function of reaction time t for nanosized and microsized catalysts at a polymerization temperature of 50°C. It can be clearly seen from Figure 1 that the nanosized catalyst produced significantly more PP than the microsized catalyst did.

Table I compares the polymerization rate [R_p (kilograms of PP produced per hour per gram of catalyst)] as a function of the reaction time for the two catalysts. The results in Table I indicate that the R_p values of the nanosized catalyst were more than 2 times the corresponding rates of the microsized catalyst. For both catalysts, the rates at $t \leqq 0.5$ h were smaller than the rates at 0.5 h $\leqq t \leqq 1$ h, and this

TABLE I
Effect of the Reaction Time on R_p

Time range (h)	0–0.5	0.5–1	1–2
R_p for the nanosized catalyst (kg of PP/h g of catalyst)	0.152	0.214	0.119
R_p for the microsized catalyst (kg of PP/h g of catalyst)	0.064	0.106	0.049

Polymerization temperature = 50°C; R_p = polymer weight produced/(time interval × catalyst weight used).

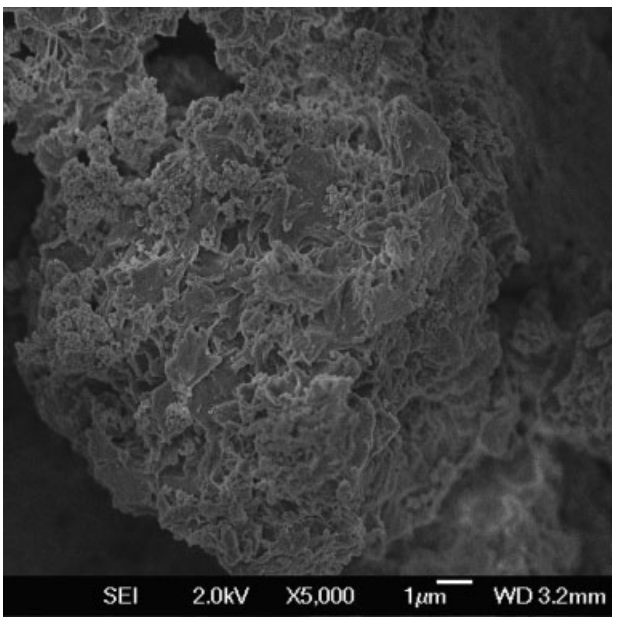

Figure 2 SEM micrograph of PP particles produced with the nanosized catalyst (polymerization time = 30 min).

should be due to the occurrence of an induction period at $t \leqq 0.5$ h.[17]

Figures 2 and 3 show SEM pictures of PP particles produced with the nanosized catalyst at $t = 0.5$ h and $t = 2$ h, respectively. The polymer particle morphology in Figure 2 ($t = 0.5$ h) is quite different from that in Figure 3 ($t = 2$ h). In Figure 2, polymer particles are aggregated together and form a aggregate with a nearly spherical shape. In Figure 3, polymer particles are separated from one another and are presented as tiny, discrete particle forms with similar sizes and shapes. Most polymer particles in Figure 3 have a length of approximately 2 μm, which is about 200 times that of the original silica particles (length ~ 10 nm[21]). The similarity of the polymer

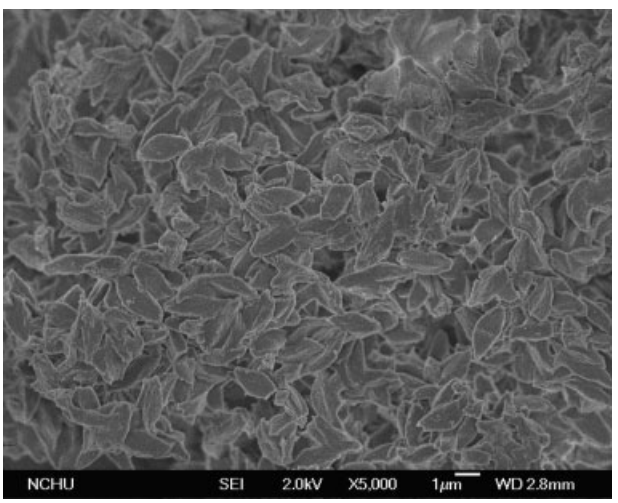

Figure 3 SEM micrograph of PP particles produced with the nanosized catalyst (polymerization time = 2 h).

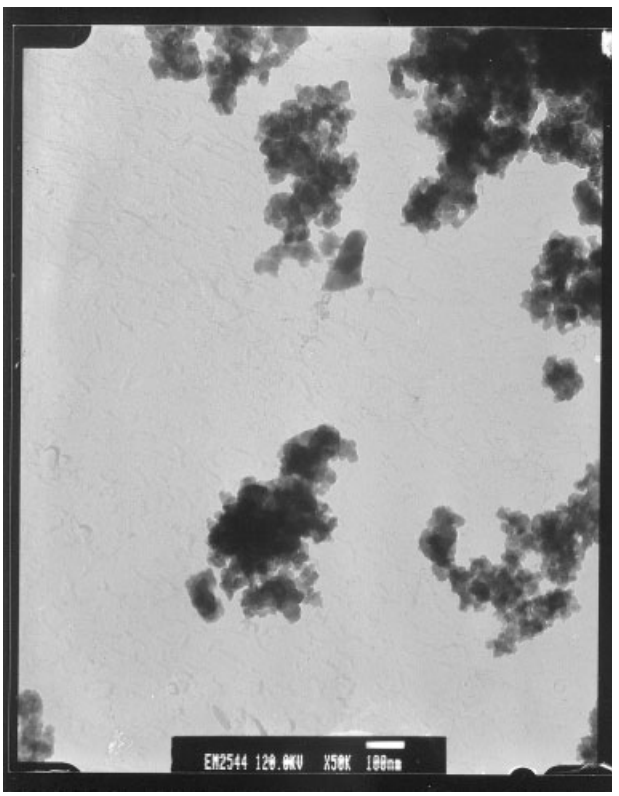

Figure 4 Transmission electron micrograph of the nanosized-silica-supported $Me_2Si(Ind)_2ZrCl_2$ catalyst.

particle sizes and shapes in Figure 3 suggests that each nanosized catalyst had uniform catalytic activity.

A transmission electron micrograph (shown in the previous article[21]) indicated that the original silica particles (before catalyst preparation) had a length of approximately 10 nm and a width of 2–4 nm. After catalyst preparation, the nanosized-silica-supported $Me_2Si(Ind)_2ZrCl_2$ catalyst had a tendency to aggregate, and each aggregate consisted of a large number of catalyst particles, as shown in Figure 4 (the catalysts are shown in the dark area of the transmission electron micrograph). The polymer chains initially produced within the catalyst aggregated to form a nearly spherical polymer aggregate, as shown in Figure 2. The catalyst aggregates then disintegrated into individual catalyst particles with further propylene polymerization, and each catalyst particle produced a discrete polymer particle with a length of approximately 2 μm, as shown in Figure 3. Therefore, a PP aggregate in Figure 2 is much larger than an individual PP particle in Figure 3.

The polymerization time was found to have little effect on the polymer molecular weight produced with the nanosized catalyst (M_v = 40,295, 40,865, and 40,193 g/g mol at t = 0.5, 1, and 2 h, respectively). With a microsized catalyst, Zechlin et al.[17] found that the weight-average molecular weight (M_w) of PP decreased significantly with increasing polymerization time. They proposed that the monomer concentration at the active centers decreased with progressive polymerization (because monomer diffusion was decreased markedly), and this resulted in a decrease in the polymer's molecular weight and melting point. The results that we obtained here (insensitivity of the molecular weight to the polymerization time) suggest that the monomer concentration and chain-transfer constant were nearly constant (independent of the polymerization time) at the active centers of the nanosized catalyst.

Catalyst characterization

Inductively coupled plasma measurements indicated that the Zr contents were 1.91 and 1.46 wt % for the nanosized and microsized catalysts, respectively. The Al contents were 7.15 and 4.43 wt % for the nanosized and microsized catalysts, respectively. The higher Zr and Al contents of the nanosized catalyst should be due to its larger surface area. BET measurements indicated that the nanosized silica had a surface area of 582 m^2/g, which was about 2 times that of the microsized silica (surface area = 305 m^2/g).

As reported earlier, nanosized silica had a slender shape with a length of 10 nm and a width in the range of 2–4 nm. By assuming that it was a cylindrical particle with a length (L) of 10 nm, a diameter (D) of 4 nm, and a density (ρ) of 2.3 g/cm^3, we calculated the specific external surface area (S_{ex}) of nanosized silica to be 520 m^2/g, using the equation $S_{ex} = [2(D^2/4) + DL]/[\rho LD^2/4]$. The calculated S_{ex} value was about 90% of the total surface area (582 m^2/g) measured with the BET method. Therefore, most of the nanosized silica surface area was external surface area, and active sites on the nanosized catalyst external surface should be free from internal diffusion resistance. An SEM micrograph (shown in the previous article[21]) indicated that microsized silica had a size of approximately 100 μm. By assuming it was a spherical particle with D = 100 μm and ρ = 2.3 g/cm^3, we calculated S_{ex} of microsized silica to be 0.026 m^2/g (using the equation $S_{ex} = 6/[\rho D]$), which was only 0.0085% of the total surface area (305 m^2/g) measured with the BET method. Therefore, almost all of the microsized silica surface area was internal (i.e., inside the pores) surface area, and active sites on the microsized catalyst internal surface should have strong diffusion resistance.

Effect of the polymerization temperature

Figure 5 shows the polymerization activity as a function of the polymerization temperature and indicates that the nanosized catalyst had significantly better polymerization activity than the microsized catalyst

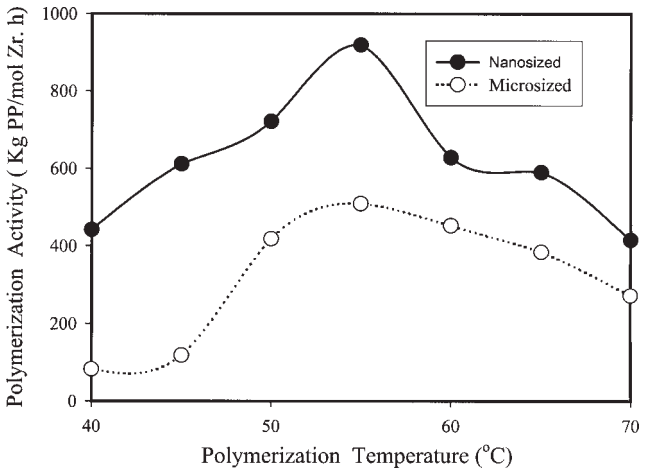

Figure 5 Polymer activity as a function of the polymerization temperature for the nanosized and microsized catalysts (polymerization time = 2 h). The Al/Zr ratios were 325 and 425 for the nanosized and microsized catalysts, respectively.

in the temperature range of 40–70°C. Both curves in Figure 5 exhibit a volcano shape with a maximum polymer activity at 55°C. The maximum polymerization activities were 919 and 509 kg of PP/mol of Zr h for the nanosized and microsized catalysts, respectively. The former was 1.8 times the latter.

R_p is generally expressed by[18]

$$R_p = k_p[C^*][M]^n \qquad (1 < n < 1) \tag{1}$$

where k_p is the propagation rate constant, [C*] is the concentration of catalytically active species C*, [M] is the monomer concentration, and n is the reaction order. Therefore, the observed polymerization activity (shown in Fig. 5) was determined by k_p, the C* concentration, and the monomer concentration (i.e., propylene solubility in toluene). The volcano shape appearing in Figure 5 was caused by the contradictory effects of temperature on k_p, the C* concentration, and the monomer concentration. It is known that the solubility of propylene in toluene decreases linearly with an increase in the temperature.[24] The C* concentration in eq. (1) is related to the material balance of all zirconocene species according to the following equation:[25]

$$[C^*] + 2[C2] + [C - MAO] + [C_d] = [Zr] \tag{2}$$

where C2 and C-MAO are two types of inactive species that are in dynamic equilibrium with C* and C_d is the dead species resulting from irreversible catalyst deactivation. With the increase in the polymerization temperature, k_p increased, but both the monomer concentration and C* concentration decreased. When the polymerization temperature was $\leqq$55°C, k_p increased more rapidly than the decrease of the C* concentration and monomer concentration, and this resulted in the increase of the observed polymerization activity. When the polymerization temperature was above 55°C, the extents of the C* concentration and monomer concentration decrease were more profound than the extent of the k_p increase, and this resulted in the decrease of the observed polymerization activity, as shown in Figure 5.

Figure 5 indicates that the nanosized catalyst had greater R_p than the microsized catalyst, and this is consistent with the results shown in Figure 1 and Table I. There are four possible reasons responsible for the higher rate observed with the nanosized catalyst: (1) the nanosized catalyst had a higher monomer concentration at the active sites because of the elimination of internal diffusion resistance, (2) the nanosized catalyst had a higher C* concentration because some of the microsized catalyst's internal active sites were not accessible to propylene, (3) the nanosized catalyst had a much higher surface area and therefore a much higher concentration of effective active sites, and (4) the nanosized catalyst might have a higher value of k_p. Reasons 1 and 2 were caused by the fact that the nanosized catalyst's active sites were located at the external surface, whereas the microsized catalyst's active sites were located inside the pores.

For propylene polymerization over supported metallocene/MAO catalysts, Bonini et al.[16] proposed a kinetic model based on the following three levels of diffusion resistance for the monomer: (1) external film surrounding the growing particle, (2) macroparticle level (the monomer diffuses inside the pores among microparticles), and (3) microparticle level (the monomer diffuses in an amorphous polymer phase as far as the catalyst surface, where the reaction takes place). The results that we obtained here (the nanosized catalyst had a higher polymer yield than the microsized catalyst) suggest that the level 2 diffusion resistance was significant for the microsized catalyst, which was a macroparticle and contained many microparticles. The microparticles were generated from fragmentation of the macroparticle.

For heterogeneous catalytic reactions, an internal diffusion effect can be evidenced by a difference in the reaction rates for the reaction over two differently sized catalyst particles.[26] Our experimental data showed that the nanosized catalyst had higher polymerization activity than the microsized catalyst. The observed difference in the polymerization activity for the two catalysts evidences that the microsized catalyst had internal diffusion resistance.

Polymer characterization

Figure 6 shows polymer M_v as a function of the polymerization temperature. At a polymerization tem-

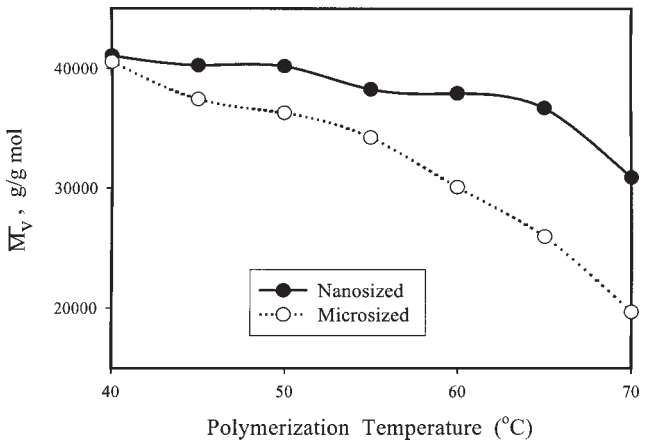

Figure 6 Effects of the polymerization temperature on M_v of the polymer.

perature greater than 40°C, the nanosized catalyst produced PP with a significantly higher molecular weight than that produced with the microsized catalyst, and the M_v difference between them increased rapidly with increasing polymerization temperature. At a polymerization temperature of 70°C and an Al/Zr ratio of 325, PP produced with the nanosized catalyst had M_v = 30,914 g/g mol, which was close to M_w of PP (36,000 g/g mol) obtained with a homogeneous $Me_2Si(Ind)_2ZrCl_2$/MAO catalyst at a polymerization temperature of 70°C and an Al/Zr ratio of 15,000.[8]

For a homogeneous $Me_2Si(Ind)_2ZrCl_2$/MAO catalyst, it was proposed that[27]

$$1/P_n = (k_{TM}/k_p)(1/[\mathrm{M}]) + k_{TO}/k_p \quad (3)$$

where P_n is the degree of polymerization [number-average molecular weight (M_n)/propylene molecular weight], [M] is the monomer concentration, k_{TM} is the chain termination rate constant due to β-H transfer to the metal, and k_{TO} is the chain termination rate constant due to β-H transfer to an olefin. Equation (3) indicates that the higher the monomer concentration is, the higher the molecular weight is of the polymer produced. Therefore, the higher molecular weight observed for the polymer produced with the nanosized catalyst (shown in Fig. 6) should be caused by the higher monomer concentration at the active sites of the nanosized catalyst. As mentioned previously, the nanosized catalyst's active sites were located at the external surface and had no internal diffusion resistance; most of the microsized catalyst's active sites were located inside the pores and had strong internal diffusion resistance. Therefore, the active sites on the nanosized catalyst had a higher monomer concentration than the internal active sites on the microsized catalyst and thus produced a polymer with a higher molecular weight.

Figure 6 also indicates that the polymer molecular weight difference between the nanosized catalyst and microsized catalyst increased rapidly with the increase in the polymerization temperature. The results suggest that the monomer concentration at the internal active sites of the microsized catalyst decreased more rapidly with increasing polymerization temperature. This was caused by the fact that the diffusion step became more important than the reaction step when the polymerization temperature was increased because k_p is more temperature-sensitive than diffusivity.

Figure 7 shows the effect of the polymerization temperature on the melting point of the polymer for the nanosized and microsized catalysts. The melting points were obtained from DSC measurements. At a polymerization temperature of 40°C, the melting point of the polymer produced with the nanosized catalyst (147.1°C) was about the same as that produced with the microsized catalyst (147.7°C), and this is consistent with the molecular weight results shown in Figure 6 (at a polymerization temperature of 40°C, M_v was 41,069 and 40,569 g/g mol for the former and latter, respectively). When the polymerization temperature was between 45 and 65°C, the nanosized catalyst produced a polymer with a higher melting point than that produced with the microsized catalyst, and this should be primarily due to the higher molecular weight of the former.

At a polymerization temperature of 55°C, the microsized catalyst produced a polymer with a polydispersity index (PDI; i.e., M_w/M_n) of 3.1, and the nanosized catalyst produced a polymer with a PDI of 1.92. That is, the nanosized catalyst produced a polymer with a narrower MWD than the microsized catalyst did. In the presence of an internal diffusion limitation, even if all sites were chemically identical,

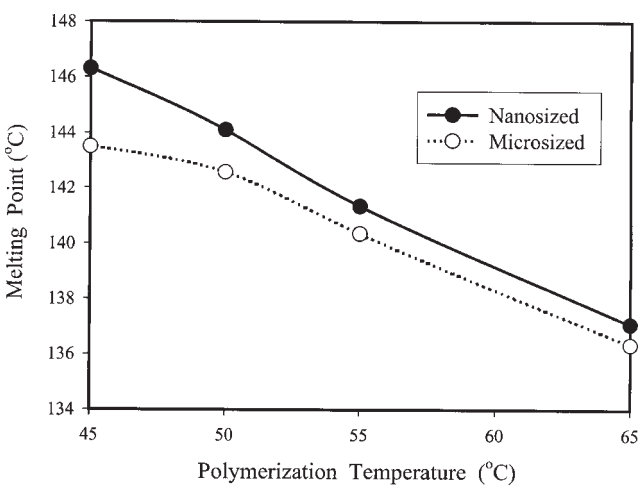

Figure 7 Effect of the polymerization temperature on the melting point of the polymer for the nanosized and microsized catalysts (polymerization time = 2 h).

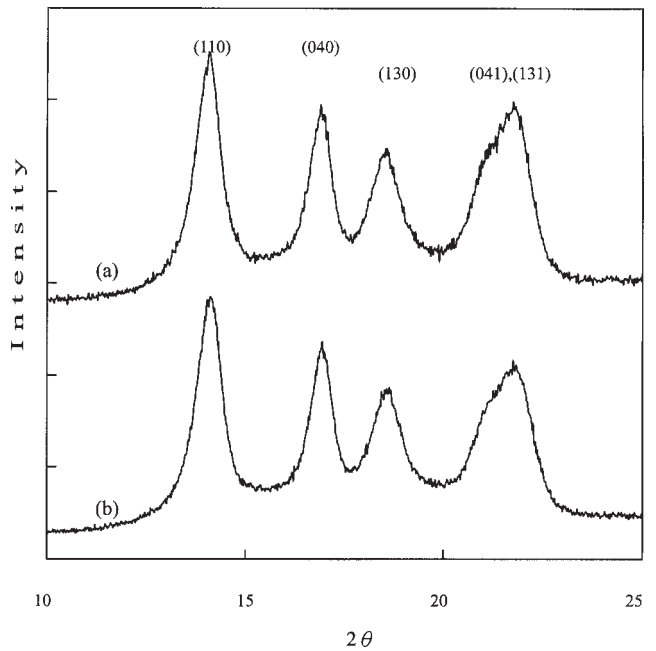

Figure 8 X-ray diffractograms of PP produced with (a) the nanosized catalyst and (b) the microsized catalyst at a polymerization temperature of 50°C.

polymer chains with different MWDs would be produced at different radial positions, and thus a rather wide overall MWD would result.[28] Therefore, the larger PDI obtained for the polymer produced with the microsized catalyst provided more evidence that the microsized catalyst had significant internal diffusion resistance.

Figure 8 displays XRD spectra of PP produced with the nanosized catalyst and microsized catalyst at a polymerization temperature of 50°C. Both spectra exhibit (110), (040), (130), (041), and (131) diffraction peaks of PP (with peak maxima appearing at 2θ values of 14.2, 17.1, 18.7, and 21.8°).[3] The patterns in Figure 8 indicate that the polymer produced was isotactic PP with a monoclinic α phase (each chain was in contact with three adjacent enantiomorphous chains and two adjacent isomorphous chains).[29,30] The similarities of the XRD spectra in Figure 8 indicate that the nanosized and microsized catalysts produced PPs with similar crystal structures. Figure 9 shows a polarized optical micrograph of PP produced with the nanosized catalyst at 55°C. An α-spherulite structure[31] is revealed in the figure with a spherulite dimension of approximately 220 μm.

Influence of metallocene

Figure 10 compares the M_v values of polymers produced with the nanosized-silica-supported $Me_2Si(Ind)_2ZrCl_2$/MAO catalyst and the nanosized-silica-supported $Et(Ind)_2ZrCl_2$/MAO catalyst, indicating that M_v of the former was more than 2 times that of the latter. In addition, the former had better isotacticity than the latter (^{13}C-NMR measurements indicated that the *mmmm* pentad concentration was 92.9% for the former and 83.7% for the latter when the polymerization temperature was 50°C). Therefore, the former had a higher melting point than the latter (e.g., at a polymerization temperature of 50°C, the melting point was 144.1°C for the former and 135.1°C for the latter). It has been proposed that the one-membered silicon bridge in $Me_2Si(Ind)_2ZrCl_2$ is preferable to the two-membered unsubstituted ethylene bridge in $Et[Ind]_2ZrCl_2$, imparting higher rigidity and favorable electronic characteristics to the metallocene and thus inducing higher isotacticity and molecular weight of the polymer.[32]

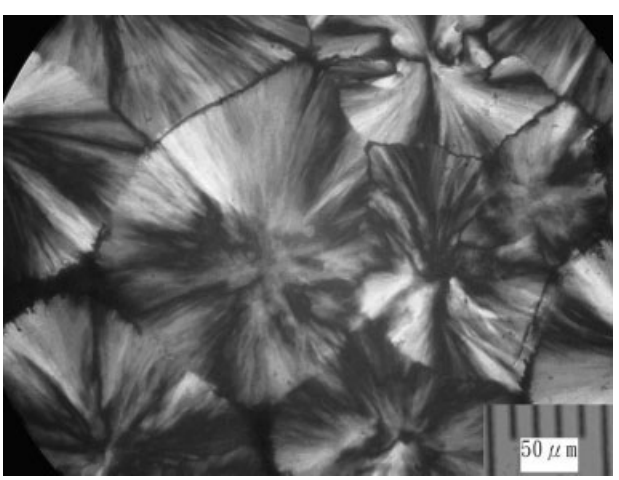

Figure 9 Polarized optical micrograph of the polymer produced with the nanosized catalyst at a polymerization temperature of 55°C and crystallized isothermally at 135°C.

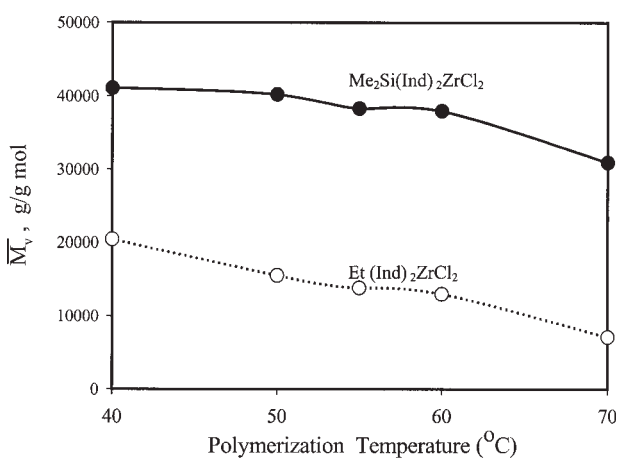

Figure 10 Comparisons of M_v of the polymer for the nanosized-silica-supported $Me_2Si(Ind)_2ZrCl_2$/MAO catalyst and nanosized-silica-supported $Et(Ind)_2ZrCl_2$/MAO catalyst.

CONCLUSIONS

A nanosized silica (whose surface area was mostly external) and a microsized silica (whose surface area was mostly internal) were used to support the catalyst $Me_2Si(Ind)_2ZrCl_2$/MAO. The effects of the silica particle size, polymerization temperature, and polymerization time on the propylene polymerization activity and polymer properties were investigated. At the optimum polymerization temperature of 55°C, the nanosized catalyst had 80% higher polymerization activity than the microsized catalyst. When the polymerization temperature was greater than 40°C, PP produced with the nanosized catalyst exhibited a significantly greater molecular weight, narrower MWD, and higher melting point in comparison with that produced with the microsized catalyst. The better performances of the nanosized catalyst were explained in terms of the higher monomer concentration at its active sites (which were located at the external surface and were free from internal diffusion resistance) and the much higher surface area. On the contrary, the microsized catalyst's internal active centers had strong internal diffusion resistance, which resulted in the lower monomer concentration and inferior performances. SEM studies showed that the nanosized catalyst produced polymer particles with similar shapes and sizes, suggesting that each nanosized catalyst particle had similar catalytic activity. XRD and optical microscopy studies indicated that the polymer produced with the nanosized catalyst was highly crystalline isotactic PP with the α form. The nanosized-silica-supported $Me_2Si(Ind)_2ZrCl_2$/MAO catalyst produced PP with a significantly higher molecular weight, isotacticity, and melting point in comparison with that produced with the nanosized-silica-supported $Et(Ind)_2ZrCl_2$/MAO catalyst.

References

1. Calamur, N. In Encyclopedia of Chemical Technology; Kroschwitz, J. I.; Howe-Grant, M., Eds.; Wiley: New York, 1996; Vol. 20, p 263.
2. Oertel, C. G. In Propylene Handbook; Moore, E. P., Ed.; Hanser: Munich, 1996; Chapter 10.
3. Lieberman, R. B.; Barbe, P. C. In Encyclopedia of Polymer Engineering and Science; Mark, H. F.; Bikales, N. M.; Overberger, C. G.; Menges, G., Eds.; Wiley: New York, 1988; Vol. 13, p 464.
4. Kaminsky, W. J Polym Sci Part A: Polym Chem 2004, 42, 3911.
5. Kaminsky, W.; Kuelper, K.; Brintzinger, H. H.; Wild, F. R. W. P. Angew Chem Int Ed Engl 1985, 24, 507.
6. Soares, J. B. P.; Simon, L. C. In Handbook of Polymer Reaction Engineering; Meyer, T.; Keurentjes, J., Eds.; Wiley-VCH: Weinheim, 2005; Vol. 1, p 380.
7. Wang, B. Coord Chem Rev 2006, 250, 241.
8. Spaleck, W.; Kuber, F.; Winter, A.; Rohrmann, J.; Bachmann, B.; Antberg, M.; Dolle, V.; Paulus, E. F. Organometallics 1994, 13, 954.
9. Soga, K.; Shiono, T. Prog Polym Sci 1997, 22, 1503.
10. Ribeiro, M. R.; Deffieux, A.; Portela, M. F. Ind Eng Chem Res 1997, 36, 1224.
11. Hlaty, G. G. Chem Rev 2000, 100, 1347.
12. Fink, G.; Steinmetz, B.; Zechlin, J.; Przyblya, C.; Tesche, B. Chem Rev 2000, 100, 1377.
13. Chien, J. C. Top Catal 1999, 7, 23.
14. Kaminsky, W.; Winkelbach, H. Top Catal 1999, 7, 61.
15. Kristen, M. O. Top Catal 1999, 7, 89.
16. Bonini, F.; Fraaije, V.; Fink, G. J Polym Sci Part A: Polym Chem 1995, 33, 2393.
17. Zechlin, J.; Steinmetz, B.; Tesche, B.; Fink, G. Macromol Chem Phys 2000, 201, 515.
18. Meier, G. B.; Weickert, G.; van Swaaij, W. P. M. J Appl Polym Sci 2001, 81, 1193.
19. Meier, G. B.; Weickert, G.; van Swaaij, W. P. M. J Polym Sci Part A: Polym Chem 2001, 39, 500.
20. Marquws, M. D. V.; Pombo, C. C.; Silva, R. A.; Conte, A. Eur Polym J 2003, 39, 561.
21. Li, K. T.; Kao, Y. T. J Appl Polym Sci 2006, 101, 2573.
22. Chien, J. C.; He, D. J Polym Sci Part A: Polym Chem 1991, 29, 1603.
23. Evans, J. M. Polym Eng Sci 1973, 13, 401.
24. Rieger, B.; Mu, X.; Mallin, D. T.; Rausch, M. D.; Chien, J. C. W. Macromolecules 1990, 23, 3559.
25. Hung, J.; Rempel, G. L. Ind Eng Chem Res 1997, 36, 1151.
26. Folger, H. S. Elements of Chemical Reaction Engineering; Prentice Hall: Upper Saddle River, NJ, 2006; p 840.
27. Stehling, U.; Diehold, J.; Kirsten, R.; Roll, W.; Brintzinger, H.; Jungling, S.; Mulhaupt, R.; Langhauser, F. Organometallics 1994, 13, 964.
28. McKenna, T. F.; Soares, J. B. Chem Eng Sci 2001, 56, 3931.
29. Philips, R. A.; Wolkowicz, M. D. In Propylene Handbook; Moore, E. P., Ed.; Hanser: Munich, 1996; p 113.
30. Manase, B.; Haudin, J. M. In Polypropylene: Structure, Blends, and Composites; Karger-Kocsis, J., Ed.; Chapman and Hall: London, 1995; Vol. 1, p 22.
31. Norton, D. R.; Keller, A. Polymer 1985, 26, 704.
32. Herrmann, W. A.; Rohrmann, J.; Herdtweck, E.; Spaleck, W.; Winter, A. Angew Chem 1989, 101, 1536.